G/T_{sys} of Prime Focus Reflector Antennas Case Study : Tantrayut's L-band Front End System with GMRT Reflector

Dr. Yogesh Karandikar
Tantrayut Telecommunications Pvt. Ltd., Ambernath, IN-421501.
website: www.tantrayut.in , e-mail: yk@tantrayut.in.

***Abstract*—This paper presents a semi-analytical approach to estimate the G/T_{sys} of the GMRT reflector given the Choke Horn Antenna as a feed along with Septum Polarizer as dual orthogonal circular polarization splitter in L-band. The analysis presented in this paper indicates that a practical GMRT reflector could achieve a Gain of $0.31 - 0.23$ (K/Jy) over the frequency range of 1050-1610MHz. And considering a practical room temperature receiver and antenna noise pickup from sky and ground, corresponding G/T_{sys} of $4.1 - 2.9 \cdot 1e^{-3}$ (/Jy) is achievable.**

This performance can be achieved by using well designed front end system components namely, 1. A Choke horn antenna which offers very high aperture efficiency of $\eta_{ap} \geq 68$ (%) over 1050 MHz to 1610 MHz for an ideal prime focus reflector with $f/D = 0.412$, 2. the Septum polarizer after the choke horn antenna which separates incoming radiation into two orthogonal circular polarized components with min of 15 dB isolation between them, 3. A carefully designed room temperature HEMT LNA which is unconditionally stable and offers a noise temperature of $T_{LNA} \leq 30$ (K) and 4. an ultra low loss ($L \leq 0.14$ dB) band pass filter which sits before the LNA to strongly reject unwanted mobile bands and to guaranty the LNA/receiver operation in linear region ($Rejection \geq 40$ dB @ $freq \leq 960$ MHz and $freq \geq 1710$ MHz).

***Index Terms*—Prime Focus Reflectors, Choke Horn, Feeds, LNA, Directivity, Polarizer, Front End System**

I. Introduction

Radio Astronomy instrumentation in L-band (1-2 GHz) is very attractive for variety of astronomical studies such as galaxy formation, extragalactic radio universe as well as pulsars. Therefore having sensitive radio telescopes in this band is highly desirable. The quality of these radio telescopes often quantified using a figure of merit which is simply a ratio of effective collecting area to the system noise temperature referred as A_{eff}/T_{sys}. However, for radio astronomy this figure of merit is slightly modified to represent it in per Jansky unit referred here as G/T_{sys}. Maximizing this figure of merit results in increasing the sensitivity of the radio telescope.

In this paper, an engineering perspective is presented to estimate G/T_{sys} for 'Giant MeterWave Radio Telescope (GMRT)' antenna using a front end system developed by 'Tantrayut Telecom (Tantrayut)' [1]. The paper uses the available engineering details of the GMRT prime focus reflector and calculates relevant aperture efficiencies when Tantrayut's front end system is used with the said reflector. Further, this paper uses semi-analytical approach to estimate the antenna noise temperature and with the knowledge of LNA/receiver temperature, calculates an effective system temperature. In this manner, the G/T_{sys} estimation over frequency bandwidth of 1050 MHz to 1610 MHz (BW_{sys}) is presented in this paper.

At first the details along with block diagrams of the Tantrayut's Front End System are presented in section II, followed by detail analysis of GMRT reflector with Choke Horn Antenna as a feed in section III. The non-uniformity and surface errors of the reflector are treated in section IV. The details of the other system components are presented in sections V-VIII. Finally the estimation of antenna temperature is presented in section IX and corresponding calculations of G/T_{sys} are presented in section X. The paper concludes by predicting ON-Source to OFF-Source Deflections for two standard Calibrator Sources namely CygA and CasA for GMRT Antenna.

II. Details of Tantrayut's Front End System

The L-band front end system developed by Tantrayut, comprises of a Choke Horn Antenna having its directivity ≈ 10.5 dBi as a feed for a prime focus reflector. Followed by the choke horn, a Septum Polarizer is used to separate two orthogonal circular polarizations in to Right Hand (RHCP) and Left Hand (LHCP) respectively. The outputs from two orthogonal polarizations are first filtered out using an ultra low loss interdigital band pass filters. The main purpose of these filters is to strongly reject mobile signals which are potential candidates for receiver saturation and undesirable spurious generation. The rejection offered by this filter is ≥ 40 dB @ $freq \leq 960$ MHz and $freq \geq 1710$ MHz thus ensuring sufficient attenuation to mobile bands while maintaining a low insertion loss ($L \leq 0.14$ dB) in passband of 1050 MHz to 1610 MHz. The block diagram of this system in shown in Fig.1.

Post filtering, directional couplers are added for noise injection and further the signal is amplified using discrete transistor (HEMT) based Low Noise Amplifiers. In reality the directional coupler and LNA are integrated on a single RF board to minimize losses before LNA. The three stage LNA offers a gain of 40 dB with +/-1dB flatness and noise temperature not exceeding 30K in the defined system bandwidth (BW_{sys}). The LNA is controlled via a digital bias board which applies required Gate and Drain bias to the transistors of the LNA and also monitors the current consumption of LNA.

Post amplification the system has digitally switchable filter bank with six discrete narrow band pass filters each having

100 MHz bandwidth. The filters can be selected by applying control bits to the appropriate RF switches. Also a white noise source is present inside the system to inject calibrated noise before the LNA. The entire system is controlled by a central microcontroller unit which communicates over ethernet protocol to the external world. Thus the system comes with only four discrete connectors (DC, RHCP, LHCP, ethernet) as an external interface.

III. Choke Horn Antenna as a Feed For Reflector

The choke horn antenna comprises of a circular waveguide input and concentric quarter wavelength deep chokes/corrugations around it. The period of chokes is typically 0.1-0.2λ. This horn when fed with fundamental TE_{11} mode of circular waveguide, generates highly rotationally symmetric far-field radiation pattern with directivity around 10 dBi. This horn also offers excellent cross-polar performance and near constant beamwidths over 1.8:1 frequency bandwidths [2]. The main advantage of using this horn is its $180°$ wide flare angle. This makes it's corrugations parallel to the feeder circular waveguide and its manufacturing becomes simplified using CNC Lathe techniques.

This choke horn has been redesigned and optimized for GMRT reflector having it's $f/D = 0.412$ and diameter of 45m. A realistic CAD model of this horn is shown in Fig.2 and its simulations has been carried out using commercial 3D EM solver 'WIPL-D Pro' [3].

The main advantage of using a choke horn is its highly rotationally symmetric beam. This rotational symmetry in the beam pattern is quantified using a term 'BOR_1' efficiency and a well designed choke horn often exhibit η_{BOR1} exceeding 99.0% [4]. This efficiency is plotted over BW_{sys} in Fig.3a. Also this horn has excellent cross-polar performance with peak cross-polar sidelobes in $\phi = 45°$ plane far-field pattern not exceeding $-25dB$. This results in very high polarization efficiency which is also plotted in Fig.3a.

The taper offered by this at the edge of the reflector (@ an angle $\theta_0 = 62.5°$) varies between -12.5 to -14.5dB. The increasing edge taper for higher frequencies in fact helps to improve the G/T_{sys} of GMRT reflector. This is due to the fact that reflector shape is achieved by metallic wire mesh which has tendency to leak more at higher frequencies which in turn increases ground noise pickup (detail treatment on this is presented in next section). This is an added argument in support of the choke horn designed by 'Tantrayut' which offers increasing taper over the frequency bandwidth. The taper as well as peak cross-polar performance of the said horn are plotted in Fig.3b.

With high BOR1, polarization and phase efficiencies, the overall aperture efficiency achieved by using a choke horn with GMRT reflector is then mainly a product of classical spillover and illumination efficiencies [5]. These efficiencies are plotted in Fig.3c and it can be observed that choke horn achieves a minimum aperture efficiency of 65% over BW_{sys} for an ideal prime focus reflector having $f/D = 0.412$ and the decrease in aperture efficiency at higher frequencies is mainly due to decreasing illumination efficiency.

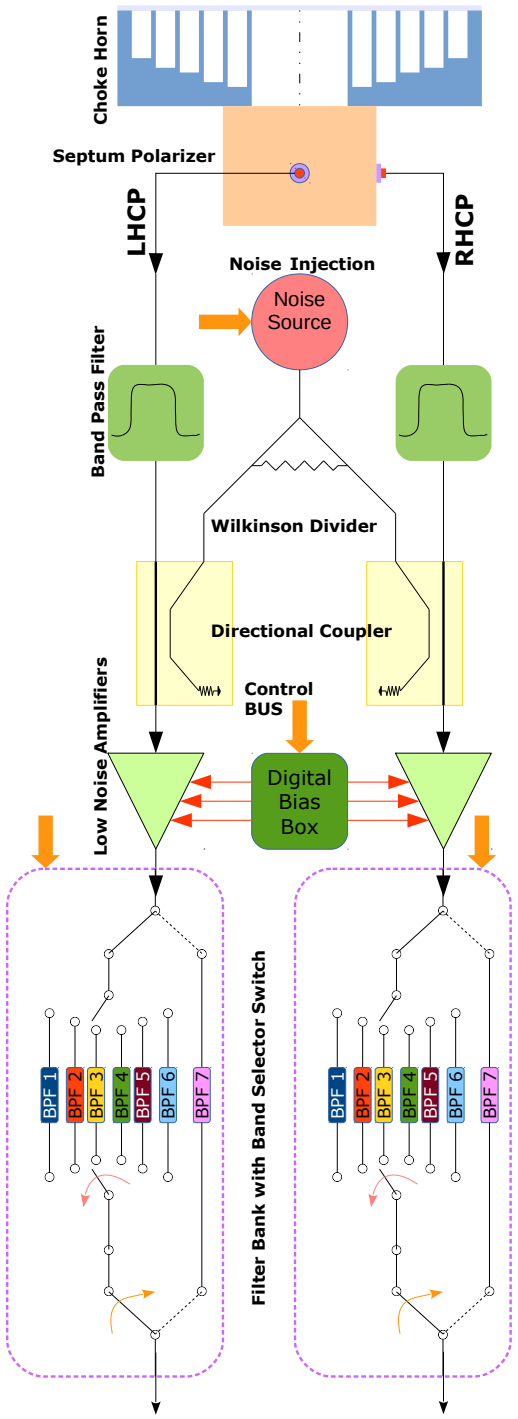

Fig. 1: Block Diagram of L-band Front End System

Another advantage of this choke horn is its near constant phase center close to its aperture as plotted in Fig.3d [6], [7]. The maximum deviation is ≈ 15 (mm) from the average phase center of 45 (mm). Thus phase center variation normalized to the wavelength of operation is less than 0.1λ. This results in negligible defocussing loss and very high phase efficiency

($\geq 99\%$) as plotted in Fig.3a. And finally the input reflection coefficient of the choke horn antenna stay below -15 dB over the required bandwidth thus making this design a robust feed solution for GMRT Reflector in L-band.

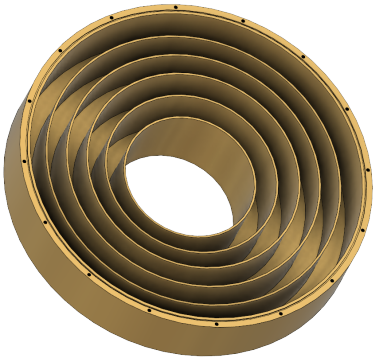

Fig. 2: 3D CAD Model of Choke Horn Antenna

IV. Surface Errors and Blockage Effects

Even though the aperture efficiency offered by Choke horn exceeds 65%, it is calculated assuming an ideal reflector. However, in reality the reflector surface deviates from ideal paraboloid which increases phase errors and hence decreases overall system aperture efficiency. Therefore, the non-uniformities of the reflector surface need to be taken into account. In case of GMRT reflector, it is fabricated using metallic wire mesh. Therefore, the reflector surface also exhibits leaky behavior. This also needs to be modeled and loss due to mesh leakage needs to be taken into account while estimating system's aperture efficiency.

The GMRT reflector has three different mesh sizes in three different parts of the reflector, namely 1. inner, 2. middle and 3. outer. The inner, middle and outer regions of the reflector are defined using a range of radial coordinate ρ and their ranges are $\rho_{inner} = 0 - 7.5$ m, $\rho_{middle} = 7.5 - 15$ m and $\rho_{outer} = 15 - 22.5$ m respectively. These mesh regions can also be defined using an angular coordinate θ_2 , θ_1 and θ_0 starting from the optical axis of the reflector. Based on this definition, the inner region is in between $\theta = 0^\circ$ to $\theta \leq 22.87^\circ$, the middle region is in between $\theta = 22.87^\circ$ to $\theta \leq 44.05^\circ$ and outer region is in between $\theta = 44.05^\circ$ to $\theta \leq 62.498^\circ$ respectively. The mesh is made up of SS wire having its diameter of $\Phi_{wire} = 0.55$ mm and the spacing (Δ) between mesh wires which is 10 , 15 and 20 mm for inner, middle and outer part respectively.

The leakage due to the mesh can be treated by first estimating the reflection coefficient of a wire grid using formulas presented in [8] and the corresponding reflector mesh efficiency η_{mesh} is then calculated as weighted average of the far-field pattern of the feed with different reflection coefficients of three different regions. These efficiencies are defined by following integrals (1). Here it is important to note that the efficiency integrals are one dimensional and therefore the extracted co-polar BOR_1 feed pattern in $\phi = 45^\circ$ plane is used for calculations. The numerical evaluations of these integrals gives an estimate on mesh efficiency of the reflector with Choke Horn antenna as a feed and its value ranges between $96 - 93\%$ in L-band as shown in Fig.4.

$$\eta_{mesh} = \frac{M2 + M1 + M0}{\int_0^{\theta_0} |G_{co}(\phi = 45^\circ, \theta)|^2 \sin\theta d\theta} \quad (1)$$

$$M2 = (1 - \Gamma_2) \cdot \int_0^{\theta_2} |G_{co}(\phi = 45^\circ, \theta)|^2 \sin\theta d\theta \quad (2)$$

$$M1 = (1 - \Gamma_1) \cdot \int_{\theta_2}^{\theta_1} |G_{co}(\phi = 45^\circ, \theta)|^2 \sin\theta d\theta \quad (3)$$

$$M0 = (1 - \Gamma_0) \cdot \int_{\theta_1}^{\theta_0} |G_{co}(\phi = 45^\circ, \theta)|^2 \sin\theta d\theta \quad (4)$$

$$\Gamma = \frac{1}{\left[1 + \left[\frac{2\Delta}{\lambda} \ln\left(\frac{\Delta}{\pi \cdot \Phi_{wire}}\right)\right]^2\right]} \quad (5)$$

Due to unequal mesh sizes, the surface RMS (σ) errors are also different in three different parts of the reflector. The specified value of these deviations from ideal surface are 08, 9 and 14 (mm) for inner, middle and outer region respectively [9]. Similar treatment can be applied to the non-uniformities of the reflector surface. Any deviation from the true paraboloid surface causes phase errors over the aperture and therefore the resultant surface efficiency ($\eta_{surface}$) considering the far-field pattern of the feed can be written as weighted average of phase errors using (6).

$$\eta_{surface} = \frac{S2 + S1 + S0}{\int_0^{\theta_0} |G_{co}(\phi = 45^\circ, \theta)|^2 \sin\theta d\theta} \quad (6)$$

$$S2 = \exp\left[-\left(\frac{4\pi\sigma_2}{\lambda}\right)^2\right] \cdot \int_0^{\theta_2} |G_{co}(\phi = 45^\circ, \theta)|^2 \sin\theta d\theta \quad (7)$$

$$S1 = \exp\left[-\left(\frac{4\pi\sigma_1}{\lambda}\right)^2\right] \cdot \int_{\theta_2}^{\theta_1} |G_{co}(\phi = 45^\circ, \theta)|^2 \sin\theta d\theta \quad (8)$$

$$S0 = \exp\left[-\left(\frac{4\pi\sigma_0}{\lambda}\right)^2\right] \cdot \int_{\theta_1}^{\theta_0} |G_{co}(\phi = 45^\circ, \theta)|^2 \sin\theta d\theta \quad (9)$$

The numerical computational results using (6) suggests that the surface efficiency is a dominating term above all other sub-efficiencies and its value ranges between $85 - 70\%$ over 1050-1630 MHz. (see Fig.4) Thus minimizing surface RMS is really important for improving G/T_{sys} of GMRT reflector. For less than 0.3 dB loss due to surface RMS (i.e. $\eta_{surface} \geq 93.3\%$) it is recommended to to achieve surface rms better than $\lambda/50$ (see Chap 9 of [10]). Therefore, for highest frequency of 1630 MHz, the surface RMS needs to be less than 3.7 (mm).

Finally, the blockage due the feed support struts and feed itself can be accounted for the loss in aperture efficiency. Here, the blockage due to the struts as well as from the feed is combined together as an effective central blockage. The reason being the complex nature of struts of GMRT with multiple truss supports on each of the four legs. Such structure could only be analyzed accurately by a Method of Moment based EM analysis.

In this paper, therefore the increased central blockage of $1/10^{th}$ reflector diameter is assumed which results in 4.5m of

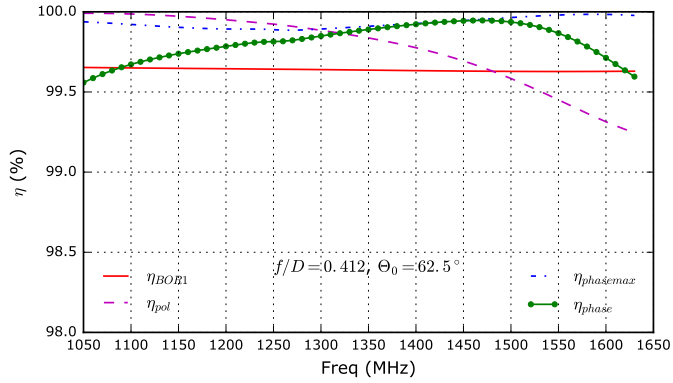

(a) BOR_1 efficiency of Choke Horn Antenna

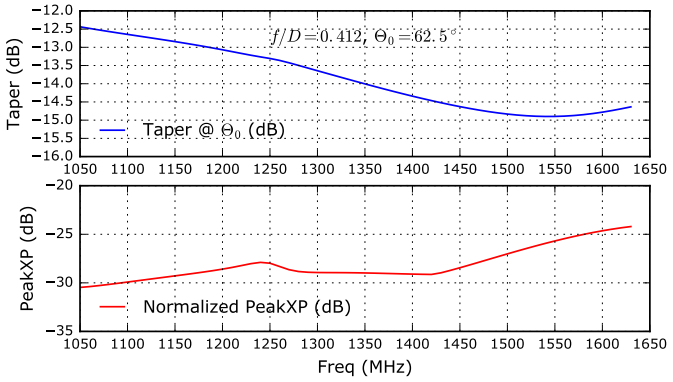

(b) Taper offered by Choke Horn Antenna @ edge of GMRT reflector

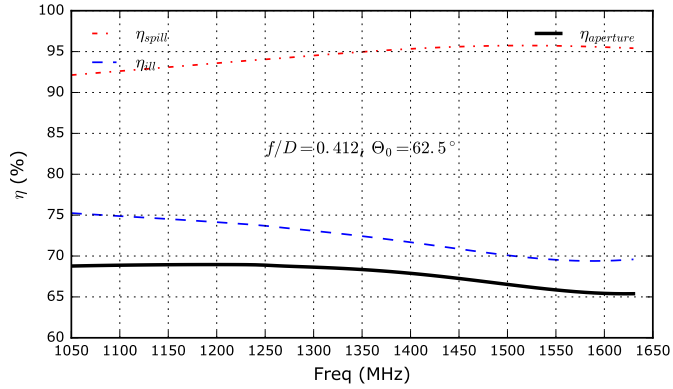

(c) Spillover and Illumination Efficiencies of the Choke Horn

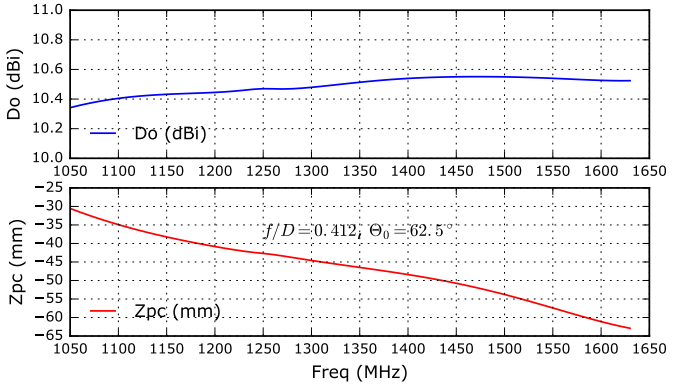

(d) Directivity and Phase center of the Choke Horn

Fig. 3: Choke Horn Performance Data for GMRT Reflector in L-band

blockage diameter. This blockage diameter is factor 7 more as compared to just feed blockage which has a diameter of 0.6m only. Therefore, it is assumed that this high margin would consider feed + struts blockage combined. Now the effective central feed blockage can then be treated analytically and it is computed using following formulas (10) [10]. The numerical calculations of (10) gives an average loss of $\approx 5\%$ over the L-band considering 10% aperture blockage diameter. In other words, the blockage efficiency is $\approx 95\%$ or better.

$$\eta_{blockage} = \left| 1 - C_b \left(\frac{\Phi_{block}}{\Phi_{refl}} \right)^2 \right|^2 \tag{10}$$

$$C_b = \frac{\tan^2(\theta_0/2) \cdot G_{co}(\phi = 45°, \theta = 0°)}{\int_0^{\theta_0} G_{co}(\phi = 45°, \theta) \tan(\theta/2) d\theta} \tag{11}$$

$$\eta_{total} = \eta_{BOR1} \cdot \eta_{pol} \cdot \eta_{spill} \cdot \eta_{ill} \cdot \eta_{phase} \cdot \eta_{block} \cdot \eta_{mesh} \cdot \eta_{surface} \tag{12}$$

Now, all these sub-efficiencies can be combined together to get effective system's aperture efficiency. This total efficiency is a product of all sub-efficiencies (12). This is plotted in Fig.4. It can be observed that even though the Choke Horn itself gives high aperture efficiency for ideal reflector ($\eta_{ap} \geq 65\%$) due to non-uniformities of the reflector surface the over all system's aperture efficiency gradually reduces from 55% at the lower end of 1050 MHz to 40% at the 1630 MHz. The dominating factor which causes the reduction is the high surface RMS of the reflector.

V. Septum Polarizer

Once we receive the focused radiation via choke horn, it is transformed into a guided TE_{11} mode of circular waveguide. And considering rotational symmetry of the reflector antenna as well as choke it supports infinite polarization orientations. Therefore, the field has to be sorted out in to two orthogonal components, either linear or circular.

The common ways to generate two orthogonal linear polarizations from feed horn is to use an ortho-mode transducer (OMT) [11], [12] or a Turnstile junction [13], [14]. The drawback of quadridge waveguide based OMT is it's long length (850mm in L-band) [12] while the drawback of Turnstile junction is its massive size and bulkiness in L-band. Even though both these transducer offer excellent linear orthogonal polarization splitting and high isolation between the respective polarization output ports, considering L-band radio astronomy their primary disadvantage is their huge size and high weight.

Furthermore, often for radio astronomy observations circular polarization is preferred. In case of OMTs based on quad ridge horn or turnstile junction , a $90°$ passive hybrid is needed to generate circular polarization. Since no practical hybrid is ideal, the achieved polarization isolation between Right Hand

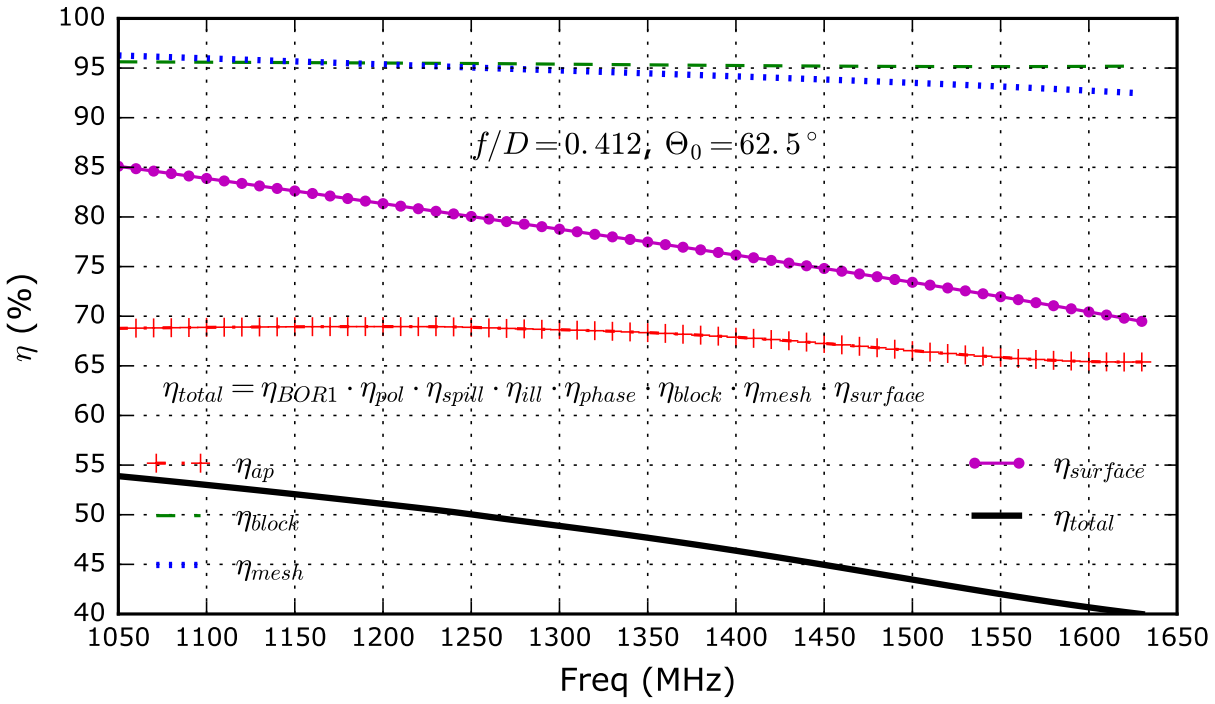

Fig. 4: Total Aperture Efficiency of GMRT Reflector with Choke Horn Feed

(RHCP) and Left Hand Circular Polarization (LHCP) depends both on the OMT and Hybrid. Further by adding a passive hybrid before a LNA increases system noise temperature while adding a hybrid post amplification introduces additional errors of gain, phase imbalance between two LNA's of orthogonal polarizations. This further degrades the RHCP to LHCP polarization isolation or increase the leakage between the two.

These disadvantages can be very much overcome by using a Septum Polarizer [15], [16]. Another advantage of using Septum polarizer is it's low 'I' to 'Q' leakage (below $\pm 2\%$) and its compact size [17]. Therefore for this front end system a square waveguide based Septum polarizer is chosen and its EM model with integrated Choke Horn antenna is shown in Fig.5a. As can be seen from Fig.5a the Septum polarizer has two rectangular waveguide outputs for RHCP and LHCP polarization. These ports can be excited with fundamental TE_{10} mode of rectangular waveguide and in one single EM simulation reflection at waveguide port as well as leakage between two ports can be calculated. The same simulation also calculates the far-field pattern of the choke horn when fed by a rectangular waveguide RHCP or LHCP port.

The results of these simulation are plotted in Fig.5b where the port 1 refers to RHCP port and port 2 refers to LHCP port. Therefore S_{11} is the reflection at the input waveguide port and S_{21} is the polarization isolation. The input reflection stays well below -20 dB over entire BW_{sys} except at two spot frequencies at 1330 MHz and 1490 MHz. Here it is important to note that the circular as well as the square waveguide supports various degenerative modes. The fundamental TE_{10} mode of the square waveguide used in Septum polarizer is about 950 MHz and next higher order modes of TE as well as TM type do occur around 1300 MHz and 1500 MHz. The discontinuities caused by stepped ridge used in Septum polarizer causes weak excitation of these modes which eventually get radiated out. The loss of power in excitation of these higher order modes is less than 2% and this loss of power actually results in small distortion in the far-field radiation pattern of the horn as these modes propagates and eventually get radiated out from the Choke Horn (Note: Antenna being a reciprocal device, its analysis is done for Transmit case).

The isolation between orthogonal circular polarization ports also stays below -15 dB over entire bandwidth. The main advantage with Septum polarizer is that the polarizer itself dictates the isolation and other external factors such as gain , phase imbalances in hybrids and LNAs while using an OMT are completely absent in this type of solution. Therefore, the polarization isolation also stays constant through out the life of the system. To further elaborate on the combination of Septum Polarizer and Choke Horn, the 3D far-field pattern of the EM model shown in Fig.5a is shown in Fig.5c. In this pattern, the excitation is applied at the right waveguide port and computed far-field pattern is decomposed into RHCP and LHCP. As seen from Fig.5c the pattern maintains very high rotational symmetry and on-axis directivity of 10.5 dBi @ 1420 MHz. While the left hand component shown in Fig.5d of the same far-field exhibits very low peak level of -4.5 dBi with distorted pattern. This suggests that the normalized cross-polar level is about 16 dB from peak co-polar level for circular polarization. Thus it is evident that a combination of Septum Polarizer with choke horn does generate high quality orthogonal circular polarizations.

In practice, the excitation to rectangular waveguide port is

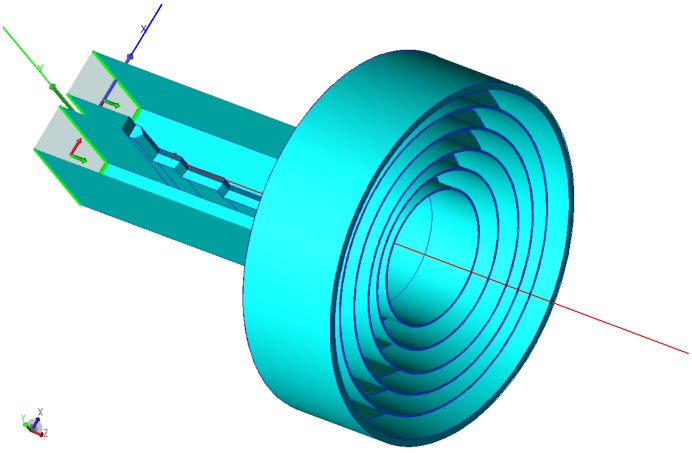

(a) WIPL-D model of Septum Polarizer with Integrated Choke Horn

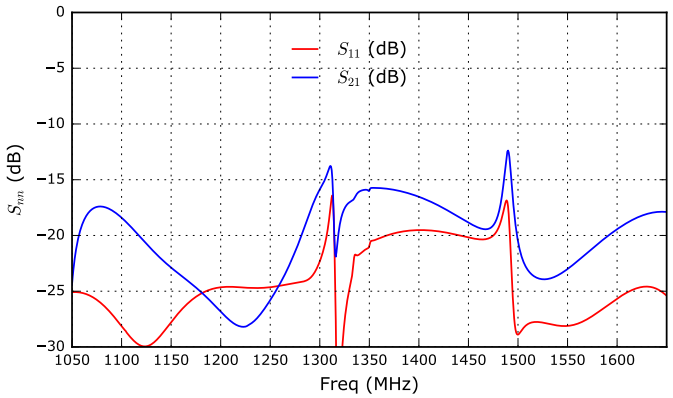

(b) Input Reflection Coefficient and Polarization Isolation of Septum Polarizer

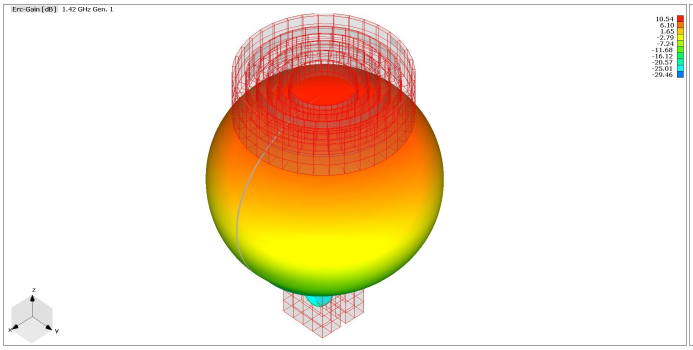

(c) RHCP Far-field pattern @ 1420 MHz

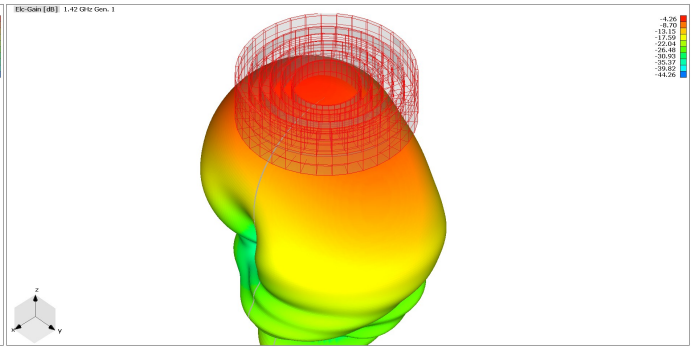

(d) Circular Cross-polarization (LHCP)

Fig. 5: Performance Data of the Choke Horn with the Septum Polarizer (co-simulations)

applied using a coaxial to rectangular waveguide transition. For Tantrayut't front end system, such transition has also been developed and mechanically integrated with the Septum polarizer such that two orthogonal circular polarizations are received over standard bluk head SMA connectors. The over all length of the said septum polarizer including waveguide to coaxial cable transition is well below 450 mm, thus making it very compact and competative alternative to classical OMT's with 90° Hybrid combinations. The complete 3D mechanical model of the said Septum polarizer is shown in Fig.6.

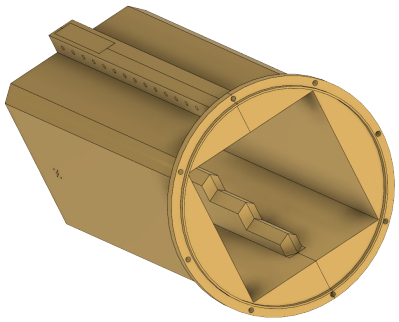

Fig. 6: 3D CAD Model of Septum Polarizer

VI. Ultra Low Loss Interdigital Band Pass Filter

The Choke Horn with Septum Polarizer mainly constitute the transition from free space EM waves to guided TEM waves in coaxial cables. The over all system bandwidth achieved by these two components is between 1050 to 1630 MHz. However these two components do also receive the radiation below 1050MHz and above 1630 MHz with degraded performance. This makes the system potentially susceptible to strong mobile Radio Frequency Interference (RFI) both from GSM and CDMA bands. The biggest concern is the power level of this RFI exceeding the saturation level of LNA (typically -40dBm @ LNA input, see section VII) which makes the system practically useless of radio astronomy observations.

Therefore, the filtering of unwanted mobile RFI is needed before the LNA. However, inserting a practical filter comes with a disadvantage that its finite insertion loss increases system temperature. This puts a requirement on filter design to minimize its insertion loss as well as achieve minimum of -40 dB stop band rejection for frequency ≤ 960 MHz and ≥ 1710 MHz.

A detail study of filter topologies suggests a use of band pass filter of type 'Interdigital' since this filter has only metallic posts inside an enclosed metallic cavity [18]. So only insertion loss is mainly associated to the surface conductivity of metal used for its fabrication and dielectric loss is absent. A 9^{th} order filter of this type is carefully designed and optimized

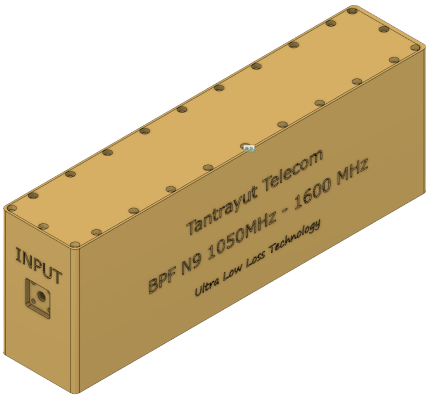

(a) 3D CAD Model of 9^{th} order Interdigital Filter

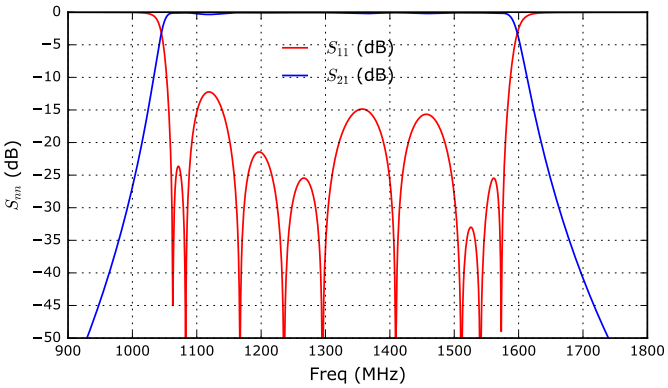

(b) S-parameters of 9^{th} order Interdigital Filter

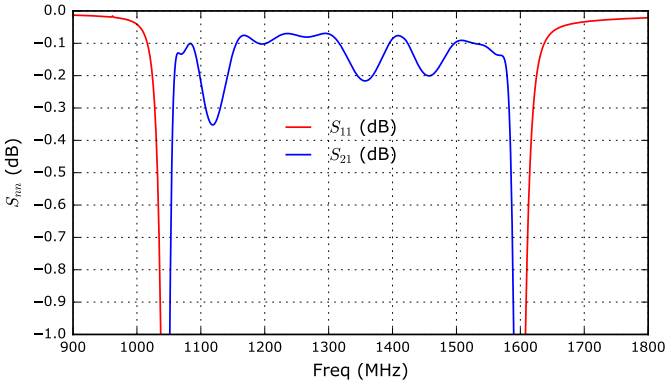

(c) Pass Band of 9^{th} order Interdigital Filter

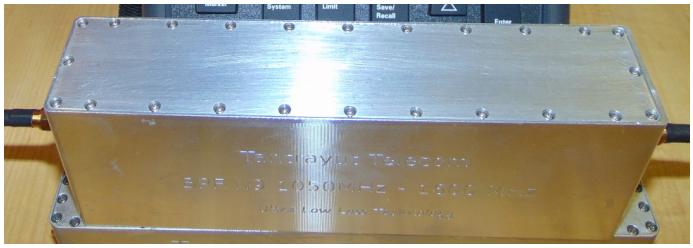

(d) Fabricated Prototype of Filter

Fig. 7: Performance Data of an Ultra Low Loss Interdigital Filter developed at Tantrayut

for this purpose. The CAD model of the said filter is shown in Fig.7a and it's realized size is only 190 x 40 x 60 mm. Thus making it highly compact for system integration. The filter comes with bulkhead SMA connectors such that it can be readily inserted between the output of Septum polarizer and LNA. The simulated S-parameters of the filter are shown in Fig.7b and details of the pass band are zoomed in Fig.7c.

It can seen from simulated s-parameters data the filter offers attenuation of $\geq$ 41 dB at frequencies below 960 MHz and $\geq$ 43 dB at frequencies above 1710 MHz. This ensures that any incoming mobile RFI is strongly attenuated before reaching the LNA and system saturation is avoided. Further by looking at the pass band carefully, as per the design the filter exhibits 0.25 dB ripple and insertion loss considering the conductivity of 22 (MS/m) is just below 0.1 dB. However considering the practical SMA connectors, the measured insertion loss of this filter module is about 0.14 dB only. This also suggests that by adding this filter before LNA, the penalty on system temperature budget is about max 10 K (see section IX). However this filter offers full immunity to mobile RFI.

VII. Directional Coupler

With filtered signal received, commonly the very next stage is to insert a Low Noise Amplifier. However considering radio astronomy receiver it is often needed to inject known , calibrated noise before LNA along with the signal. This is practically achieved by using a directional coupler.

The detail theory about directional couplers can be found in the literature [19], [20]. Therefore in this paper only the results are presented. The well designed direction coupler on a low loss RF substrate using coupled microstrip line technology offers very low insertion loss on through path ($S_{21} \geq -0.1$ dB) and excellent isolation ($S_{41} \leq -40$ dB) (see Fig.8a). Furthermore the directivity (i.e. amount of coupling from coupled to through port) can also be adjusted to achieve required deflection in system noise level with injection of noise source.

Considering commercially available white noise sources which offer 31 dB Excess Noise Ratio (ENR) , the directivity of the said directional coupler is chosen to be 24 dB. This results in about 4-5 dB deflection to system noise level between ON-OFF switching of noise source. In practice, the direcitvity S_{31} varies between -25 to -23 dB from low to high freq and also the rate ENR of the noise source varies by ± 1.5 dB, thus effectively the injected noise source level achieved ± 1 dB flatness in its spectrum over the system bandwidth of 1050-1630 MHz. The only disadvantage using this method of noise injection is increased insertion loss before LNA which in turn increases the system noise temperature.

However, considering the performance of this coupler (see Fig.8b), the low insertion loss constitutes to max 7 K increase in system noise temperature.

VIII. Low Noise Amplifier

A Low Noise Amplifier is a critical component for achieving a low system noise temperature and in radio astronomy application 'High Electron Mobility Transistor (HEMT)' based LNA undoubtedly offers lowest noise [21]. The noise temperatures achieved by these LNA's at cryogenic temperatures could reach well below 10 K [22], [23]. However considering a room temperature operation HEMT based LNAs offer typical noise temperatures between 20 to 30 K at an ambient temperature of 290 K.

In this front end system, a room temperature LNA based on commercially available discrete HEMT from 'Broadcom' is used [24]. These transistors offers moderate noise figures ($0.3 - 0.5$ dB) over L-band and a three stage based on these transistors could offer about 40 dB gain. A care has been taken in the design to achieve an excellent gain flatness of ± 0.5 dB over L-band and realized noise temperature of complete unit with Bulkhead SMA connectors does not exceed 35 K over the required system bandwidth. The Gain and Noise temperature of this LNA is shown in Fig.9a and corresponding input and output matching is shown in Fig.9b.

Another important required criterion for LNAs is it's unconditional stability. This LNA design also achieves the required condition of unconditional stability and stability factor 'k' of this LNA is plotted in Fig.9c and fabricated unit is shown in Fig.9d. The final step in LNA characterization is it's tolerance to high power levels often quantified as '1 dB compression point' (P_{1dB}). For radio astronomy perspective, it is more convenient to state P_{1dB} at the input of the LNA as this power level becomes a threshold for max tolerable RFI power levels. The measured P_{1dB} of the said LNA is -39 dBm w.r.t. input of the LNA.

Thus considering the 'Tantrayut's' front end system which incorporates an ultra low loss filter before the said LNA having -39 dBm P_{1dB} at its input and insertion loss of filter min 40 dB to both mobile bands, system becomes immune to mobile RFI as high as 0dBm. Since any mobile RFI received by the feed with its power reaching 0dBm would get attenuate below -40 dBm before getting injected into the LNA. Thus guarantying the LNA operation in linear region and stable, spurious free receiver system.

IX. Estimation of Antenna Temperature

With the knowledge of the feed radiation pattern and the geometry of the reflector antenna as covered in earlier sections, now its possible to estimate noise received by the reflector antenna. This noise estimation is based on the calculations of aperture efficiencies (presented in section III) and known sky background (galactic as well as cosmic microwave). Further considering the leaky nature of GMRT reflector , the pickup of ground noise through mesh also needs to be treated. For this estimation following assumptions are made

- Reflector Antenna is pointed towards Zenith (Elevation 90°).
- The Cosmic Microwave Background is omnipresent with noise temperature of $T_{CMBR} = 2.73$ K.
- The Galactic Background is uniform over the sky and its frequency dependence is defined by (13).
- The ground is considered as a black body with noise temperature $T_{Gnd} = 290$ K.

Based on this it is possible to estimate antenna temperature by considering the spillover efficiency of the feed. Since the spill over efficiency describes amount of power hitting the reflector, this power is likely to receive noise from the sky while the remaining power is spillover loss and hits the surrounding area. The power picked up by these spillover radiation is often expressed as an average spillover temperature and can be approximated to the physical temperature of the ground (TGnd). The addition of these two contributions results in antenna temperature and it is defined in (14). However this antenna temperature valid ideal prime focus paraboloid reflector.

$$T_{Galactic} = 20 \cdot \left(\frac{408}{\nu(MHz)} \right)^{2.75} \tag{13}$$

$$T_{Ant} = \eta_{spill} \cdot (T_{CMB} + T_{Galactic}) + (1 - \eta_{spill}) \cdot T_{Gnd} \tag{14}$$

Therefore considering GMRT reflector, the noise picked by leaky mesh needs to be added to it. The leakiness of the mesh has already been quantified as η_{mesh} (1). This mesh efficiency indicates amount of power reflected by the mesh and therefore $1 - \eta_{mesh}$ quantifies amount of power leaking through mesh. Again similar to sky noise, the spillover efficiency can be used to get a quantitative estimate for ground noise pickup through mesh using (15).

$$T_{mesh} = \eta_{spill} \cdot (1 - \eta_{mesh}) \cdot T_{Gnd} \tag{15}$$

Thus total noise contribution from GMRT reflector can be calculated as the sum of contributions from galactic background, CMBR, ground noise pick up by the primary beam of the reflector and ground noise pickup by feed directly through leaky mesh. These calculations using the simulated far-field pattern of the choke horn are perfomed and results are plotted in Fig.10.

As can be seen from Fig.10 the contribution to antenna noise due to Galactic Background and CMBR is about 4 K and its variation is ± 1 K over L-band. The dominating contribution to antenna noise is due to the direct ground noise pick up which is of the order of 15 ± 5 K and mesh leakage of similar magnitude. The noise temperature due to mesh leakage exhibits positive slope for increasing frequencies due to the fact that mesh becomes more leaky while the direct ground noise pickup decreases with increasing frequency due to the increasing edge taper offered by the Choke Horn antenna. In summary considering all these practical contributions the antenna noise in L-band is estimated to be 35 ± 5K over the system bandwidth of 1050 to 1610 MHz.

X. G/T_{sys} for GMRT Reflector

With estimation of antenna temperature, it is now possible to first calculate the system noise temperature and further

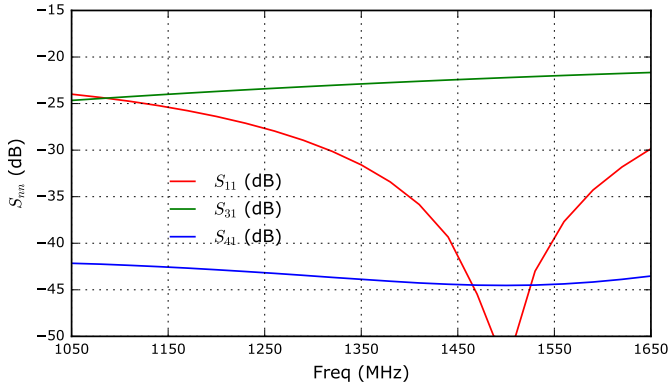

(a) Input Reflection (S_{11}), Directivity (S_{31}) and Isolation (S_{41}) of Directional Coupler

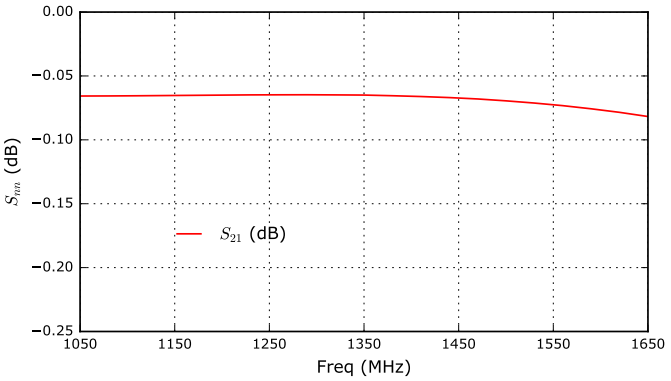

(b) Insertion Loss of Directional Coupler

Fig. 8: Performance data of Directional Coupler

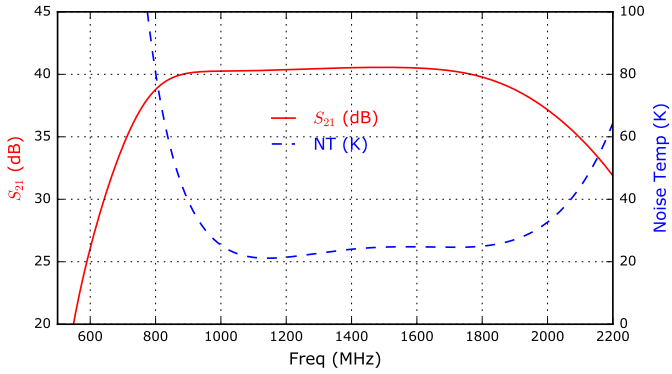

(a) LNA Gain and Noise Temperature

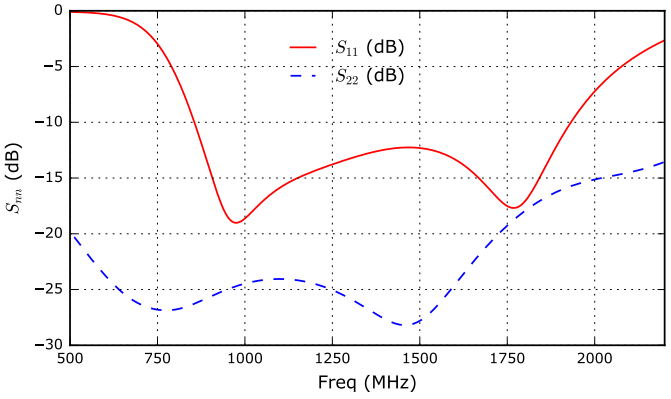

(b) Input and Output Matching

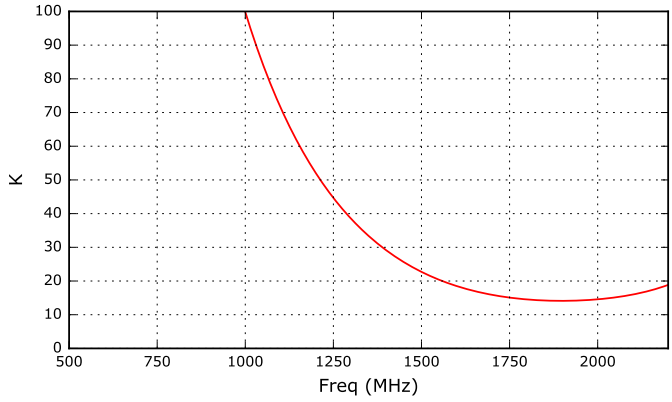

(c) Stability Factor

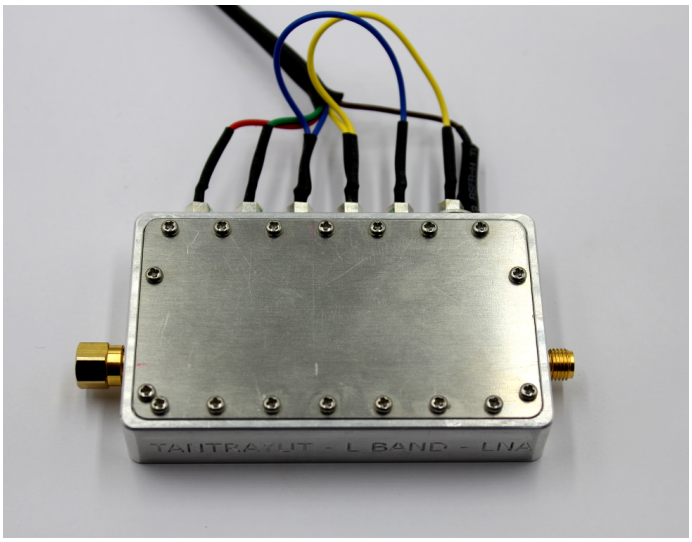

(d) Fabricated unit of LNA

Fig. 9: Performance data of Low Noise Amplifier

with the help of aperture efficiency calculations presented in section III and IV, the G/T_{sys} can be calculated. To compute the system temperature, it first required to calculate receiver temperature. The dominating part of receiver temperature is in fact noise temperature of LNA, however considering the system diagram presented in Fig.1 there are finite losses present before the LNA due to cable, band pass filter and directional coupler. These losses also contribute the system noise and therefore needs to be treated. As presented in section VI, the ultra low loss band pass filter introduces 0.14 dB insertion loss and subsequent directional coupler adds further 0.08 dB. Also in practical system there exists a short length coaxial cable ($l \leq 100$ mm) between Septum Polarizer and band pass filter. Even though short the cable also exhibits about 0.1 dB loss. Thus total loss before LNA amounts to $IL \approx 0.32$dB. Now by using Friss Formula for Noise Figure of cascaded networks, the receiver and system noise temperature can be calculated using (16),(17). This resultant system temperature is plotted in Fig.10 and it's estimated value ranges between $76-80$ K in the frequency range of 1050 MHz to 1630 MHz.

$$T_{rec} = T_{amb} \cdot \left[10^{\frac{IL_{cable}+IL_{bpf}+IL_{coupler}}{10}} - 1\right] + T_{LNA} \quad (16)$$

$$T_{sys} = T_{ant} + T_{mesh} + T_{rec} \quad (17)$$

With the knowledge of system temperature and system aperture efficiency as per (12), it is now possible to compute the Gain of a single dish radio telescope and further G/T_{sys}. Here antenna gain first needs to be expressed in terms of units of 'Kelvin per Jansky' (K/Jy) which is a measure of its sensitivity. It is defined as per the (18) [25]. Now considering GMRT reflector which is of the type prime focus paraboloid, its aperture has circular shape and therefore for a diameter of 45m, its physical area becomes $1590.43m^2$(19). This area multiplied by systems aperture efficiency gives effective area of the system which inturn gives sensitivity using (18). The system aperture efficiency considering all practical effects is already plotted in Fig.4 and therefore using its estimated value the resultant G is plotted in Fig.11. Further using the estimated values of system noise temperature (see Fig.10) the predicted G/T_{sys} is also plotted.

$$G = \frac{\eta_{total} \cdot A_{physical} \cdot 10^{-26}}{2 \cdot k_B} \quad (18)$$

$$A_{physical} = \pi \cdot D_{refl}^2/4 \quad (19)$$

As can be observed from Fig.11, the telescope Gain varies from 0.31 (K/Jy) to 0.23 (K/Jy) over the system bandwidth of 1050 to 1630 MHz. At classical 1420 MHz radio astronomy frequency its value is 0.27. The drop in gain at higher end of frequency spectrum is mainly due increasing mesh leakage of GMRT reflector and surface errors. The effective G/T_{sys} also follows similar trend and its value ranges between $4.1 \cdot 10^{-3}$ to $2.9 \cdot 10^{-3}$ over the system bandwidth.

XI. GMRT Reflector's Primary Beam Size

With estimation of Gain, it is also possible to estimate the directivity and antenna beam width by assuming uniform E-field distribution over a circular aperture having its physical area equal to the effective area (A_{eff}) of GMRT reflector. This approximation works in practice because the systems total aperture efficiency (η_{total}) is taken into account while calculating effective area and based on this area an equivalent diameter of circular aperture is computed using (20). Based on this effective diameter, the 3dB full beamwidth can be computed using known formulas from far-field of uniform circular aperture as given in (21) [10]. Similarly based on effective diameter on-axis peak directivity can be computed using (22).

The results of this calculations are plotted in Fig.12. The achieved beamwidth considering leaky mesh GMRT reflector with 'Tantrayut' Choke Horn antenna as a feed; varies between 30 to 23 arc min in L-band and corresponding peak on axis Directivity ranges between 51 to 53.5 dBi.

$$D_{eff} = \sqrt{\eta_{total} \cdot D_{refl}^2} \quad (20)$$

$$FWHM = \frac{360}{\pi} \sin^{-1}\left(\frac{0.51\lambda}{D_{eff}}\right) \cdot 60 \quad (21)$$

$$D_{max} = 20 \cdot \log_{10}\left(\pi \cdot \frac{D_{eff}}{\lambda}\right) \quad (22)$$

XII. Deflections for Calibrator Sources

The best way to measure the sensitivity of single dish radio telescope is to understand change in signal level when pointed at a particular radio source whose intensity has been well established. This change in signal level when pointed at a Calibrator Source as compared to pointed at source free region of the sky is often referred as 'On-Off Source Deflection' and it is proportional to the sensitivity of the telescope. There exist several calibrator sources of which CasA, CygA exhibit higher flux densities (1500-2700Jy) in L-band. Therefore in this section calculations are presented for CasA and CygA.

The source CasA could be treated as a point source however its flux has spectral as well as temporal variation and therefore model of CasA presented in [26], [27] has been adopted to estimate the flux of it. Once the source flux is known, the signal level at ON-Source is sum of Source flux multiplied by Gain of telescope and system noise temperature while an OFF-Source position results only in system noise. Therefore a deflection in logarithmic scale can be calculated using (23).

$$\Delta = 10 \cdot \log_{10}\left(\frac{S_\nu \cdot G + T_{sys}}{T_{sys}}\right) \quad (23)$$

The computed flux density for CasA based on the model and corresponding estimated source deflection is plotted in Fig.13. The results of these computations suggests that the deflection to calibrator source CasA varies between 10.6 dB to 8.4 dB over the system bandwidth. The resultant deflection is due to increased sensitivity and gain of the radio telescope with Tantrayut's front end system. For comparison reported gain of GMRT as per status document (as of 15 Dec 17) [28] varies between $0.28 - 0.22$ (K/Jy) over 1050 to 1450 MHz while the estimated gain is $0.31 - 0.26$ (K/Jy) over same frequency range. Further the reported system in this paper is more broadband and its gain 0.23 (K/Jy) is achieved at

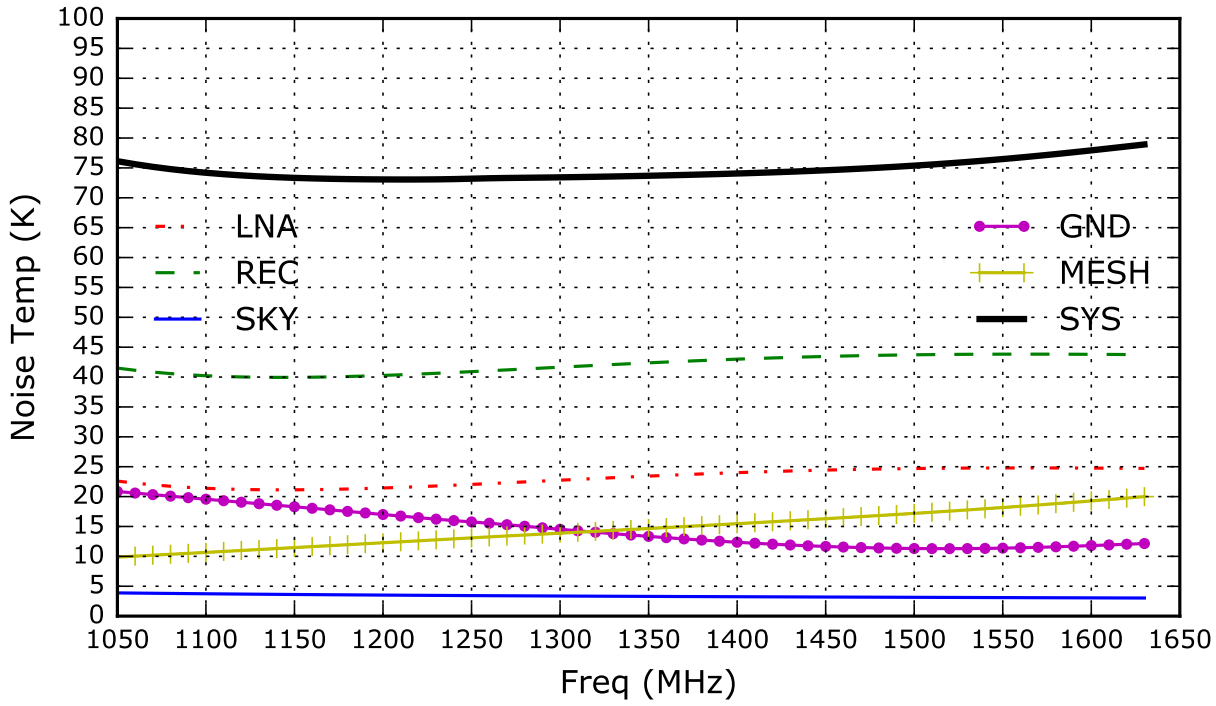

Fig. 10: Contributions to System Noise Temperatures by different factors

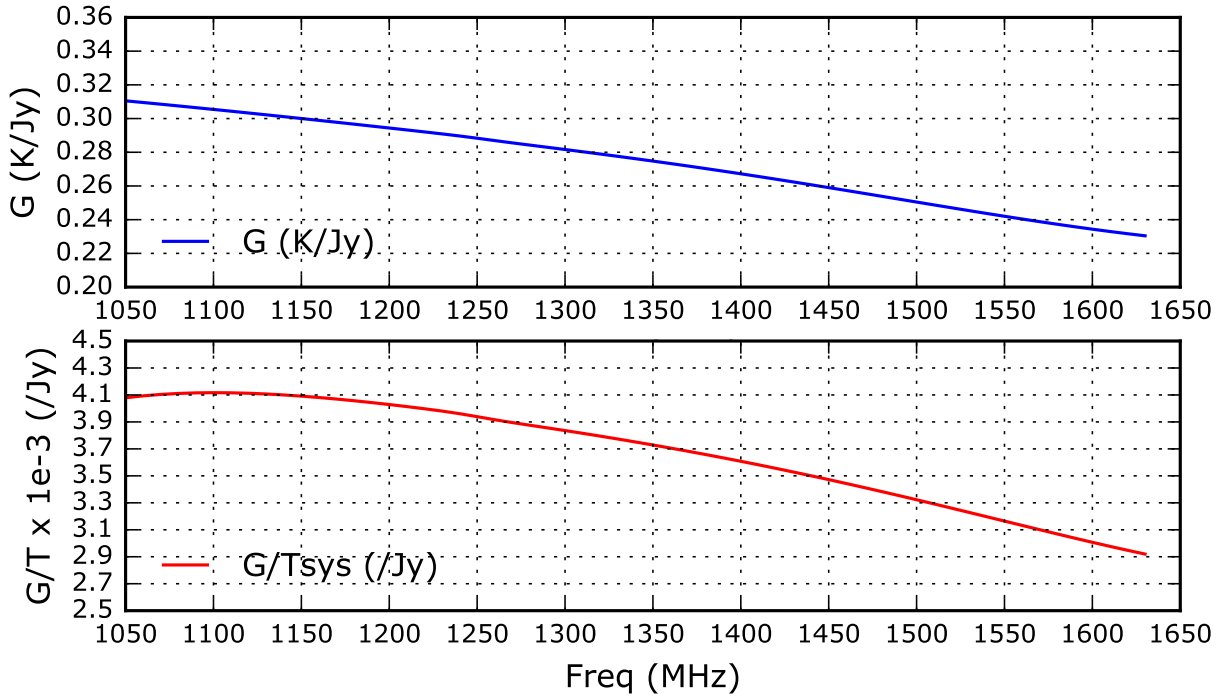

Fig. 11: Estimated GMRT Gain and Sensitivity

1630 MHz. Thus increased bandwidth performance beyond 1450MHz is practically feasible with Tantrayut's front end system.

Similar analysis can now be applied for source CygA. For this source, a third order polynomial model of source flux is used and corresponding deflection is computed [26]. The results of the computations are plotted in Fig.14. For CygA, the estimated deflection ranges between 9.7 to 6.9 dB over 1050-1630 MHz. This compared with deflection measurements of GMRT's existing front end system (as of 12 Jan 2017) [29] varies between 6-7 dB at a frequency of 1390MHz.

XIII. Conclusions

The front end system developed by 'Tantrayut' has been thoroughly discussed in this paper and its performance when used in prime focus GMRT reflector has been estimated. Considering the far-field radiation patterns of the choke horn and leaky mesh surface of GMRT reflector, the overall systems total aperture efficiency is estimated to be in the range of $55 - 40\%$ in the frequency bandwidth of 1050 MHz to 1630MHz and considering all other practical contributions to system noise, the estimated system noise temperature ranges 75 ± 3K. This translates to estimated telescope gain of $0.31-0.23$ (K/Jy) and corresponding G/T_{sys} of $4.1-2.9{\cdot}1e^{-3}$ (/Jy).

The biggest advantage in using such front end system lies in direct orthogonal circular polarization outputs from Septum polarizer and guaranteed rejection to unwanted mobile bands due to the presence of ultra low loss band pass filter.

The Septum polarizer being a passive device in waveguide technology, it ensures time invariant response of the polarization isolation or leakage. Also the polarization leakage solely depends upon the design of Septum polarizer. This approach also offers negligible contribution to system noise as compared to passive 90° Hybrid before LNA.

Furthermore, the gain and sensitivity estimates presented in this paper are rather conservative, since higher aperture blockage of (10% of reflector diameter) as well as higher ohmic losses on passive components are considered in these calculations. Therefore Tantrayut's Front End System with GMRT reflector would exhibit min $4.1 - 2.9 \cdot 1e^{-3}$ (/Jy) or better sensitivities over 1050MHz to 1630 MHz.

Also it is useful to state that the size of the said front end system is only 0.54m x 0.54m x 0.70m and its physical weight being less than 80kg. This makes the system mechanically compact and causes less loading to the focal support structure of the dish.

Acknowledgments

We thank National Center for Radio Astrophysics, TIFR for giving us an opportunity to contribute towards front end system development for 15m Radio Telescope. We would like to thank Prof. Jayaram Chengalur, Dean-NCRA and Prof. Yashwant Gupta, Center Director-NCRA for facilitating the work. We would also like to thank several engineers/researchers at NCRA-GMRT, Mr. Suresh Kumar, Mr. Pravin Raybole, Mr. Apurba Bera and Mr. Niruj Mohan for various practical discussions related to system sensitivity.

References

[1] GMRT, "Giant meterwave radio telescope," http://www.ncra.tifr.res.in/ncra/gmrt/gmrt-users/low-frequency-radio-astronomy.

[2] Z. Ying, A. Kishk, and P.-S. Kildal, "Broadband compact horn feed for prime-focus reflectors," *Electronics Letters*, vol. 31, no. 14, pp. 1114 –1115, jul 1995.

[3] WIPL-D, "Wipl-d pro cad," http://www.wipl-d.com.

[4] P. Kildal and Z. Sipus, "Classification of rotationally symmetric antennas as types bor 0 and bor 1," *Antennas and Propagation Magazine, IEEE*, vol. 37, no. 6, p. 114, Dec. 1995.

[5] P.-S. Kildal, "Factorization of the feed efficiency of paraboloids and cassegrain antennas," *Antennas and Propagation, IEEE Transactions on*, vol. 33, no. 8, pp. 903 – 908, aug 1985.

[6] ——, "Combined e - and h -plane phase centers of antenna feeds," *Antennas and Propagation, IEEE Transactions on*, vol. 31, no. 1, pp. 199 – 202, jan 1983.

[7] ——, "Comments on "phase center calculations of reflector antenna feeds"," *Antennas and Propagation, IEEE Transactions on*, vol. 33, no. 5, pp. 579 –580, may 1985.

[8] J. Chengalur and R. Kher, "Transmission through wire grids," Tata Institute of Fundamental Research, TIFR, Mumbai, Tech. Rep. 090228, 1987.

[9] GMRT, "Gmrt antenna specifications," http://www.ncra.tifr.res.in/ncra/gmrt/about-gmrt/introducing-gmrt-1/gmrt-antenna-specifications.

[10] P.-S. Kildal, *Foundations of Antennas: A Unified Approach*. Lund, Sweden: studentlitteratur, 2000.

[11] G. Valente, G. Montisci, T. Pisanu, A. Navarrini, P. Marongiu, and G. A. Casula, "A compact l-band orthomode transducer for radio astronomical receivers at cryogenic temperature," *IEEE Transactions on Microwave Theory and Techniques*, vol. 63, no. 10, pp. 3218–3227, Oct 2015.

[12] J. Fan, Y. Yan, C. Jin, D. Zhan, and J.-R. Luo, "Design of wideband quad-ridged waveguide orthomode transducer at l-band," *Progress In Electromagnetics Research C*, vol. 72, no. 10, pp. 115–122, Mar 2017.

[13] A. Navarrini and R. L. Plambeck, "A turnstile junction waveguide orthomode transducer," *IEEE Transactions on Microwave Theory and Techniques*, vol. 54, no. 1, pp. 272–277, Jan 2006.

[14] S. Srikanth, "Turnstile junction orthomode transducer," http://www.aoc.nrao.edu/evla/admin/reviews/OMT/designrevu04.pdf.

[15] J. Bornemann and S. Amari, "Septum polarizer design for antenna feeds produced by casting," in *IEEE Antennas and Propagation Society International Symposium 1997. Digest*, vol. 2, July 1997, pp. 1422–1425 vol.2.

[16] N. C. Albertsen and P. Skov-Madsen, "A compact septum polarizer," *IEEE Transactions on Microwave Theory and Techniques*, vol. 31, no. 8, pp. 654–660, Aug 1983.

[17] Y.-L. Chen, T. Chiueh, and H.-F. Teng, "A 77-118 ghz resonance-free septum polarizer," *Instrumentation and Methods for Astrophysics*, vol. 211, no. 1, p. 11, Feb 2014.

[18] M. Dishal, "A simple design procedure for small percentage bandwidth round-rod interdigital filters (correspondence)," *IEEE Transactions on Microwave Theory and Techniques*, vol. 13, no. 5, pp. 696–698, Sep 1965.

[19] D. Pozar, *Microwave Engineering*. New York, USA: John Wiley & Sons, 2004.

[20] R. Collin, *Foundations for Microwave Engineering*. New York, USA: McGraw-Hill Inc, 1992.

[21] N. Wadefalk, P.-S. Kildal, and H. Zirath, "A low noise integrated 0.3-16 ghz differential amplifier for balanced ultra wideband antennas," in *Compound Semiconductor Integrated Circuit Symposium (CSICS), 2010 IEEE*, oct. 2010, pp. 1 –4.

[22] J. Schleeh, H. Rodilla, N. Wadefalk, P. . Nilsson, and J. Grahn, "Characterization and modeling of cryogenic ultralow-noise inp hemts," *IEEE Transactions on Electron Devices*, vol. 60, no. 1, pp. 206–212, Jan 2013.

[23] J. Schleeh, N. Wadefalk, P. . Nilsson, J. P. Starski, G. Alestig, J. Halonen, B. Nilsson, A. Malmros, H. Zirath, and J. Grahn, "Cryogenic 0.5 -13 ghz low noise amplifier with 3 k mid-band noise temperature," in *2012 IEEE/MTT-S International Microwave Symposium Digest*, June 2012, pp. 1–3.

[24] Broadcom, "Single voltage e-phemt low noise 36 dbm oip3 in sc-70," https://www.broadcom.com/products/wireless/transistors/fet/atf-54143#overview.

[25] D. Campbell, "Measurement in radio astronomy," in *Single-Dish Radio Astronomy: Techniques and Applications*, vol. 278, Dec 2002, pp. 81–90.

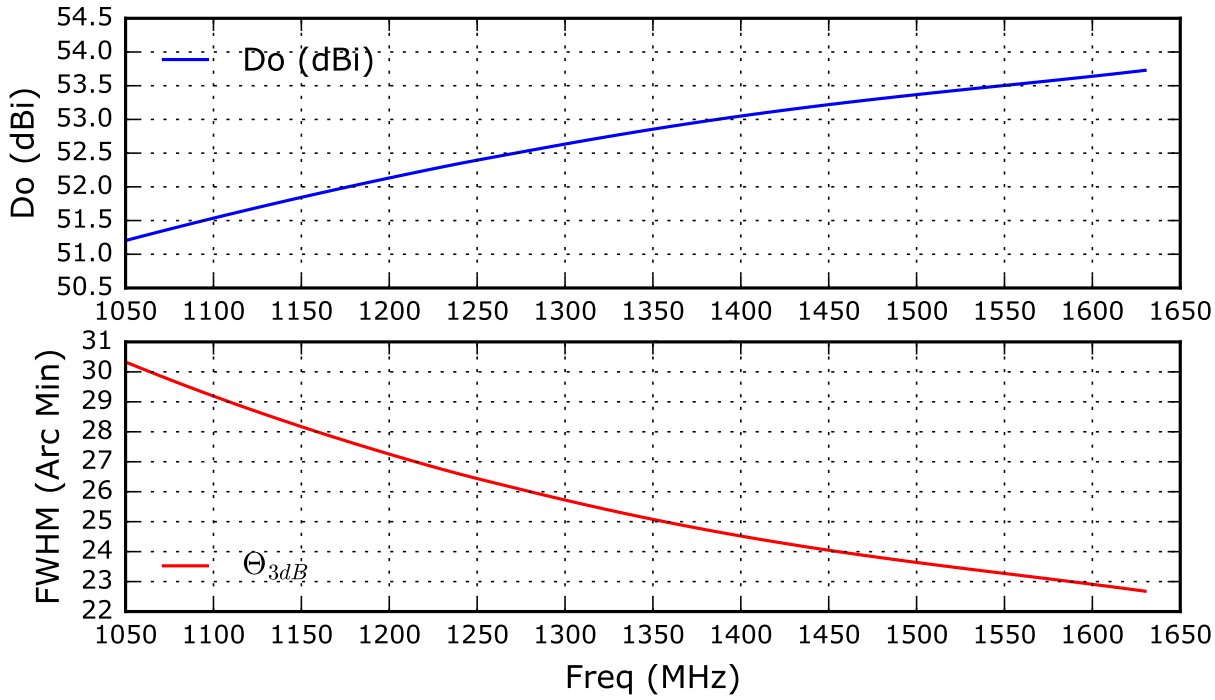

Fig. 12: GMRT antenna directivity and FWHM

[26] A. S. Trotter, D. E. Reichart, R. E. Egger, J. Stýblová, M. L. Paggen, J. R. Martin, D. A. Dutton, J. E. Reichart, N. D. Kumar, M. P. Maples, B. N. Barlow, T. A. Berger, A. C. Foster, N. R. Frank, F. D. Ghigo, J. B. Haislip, S. A. Heatherly, V. V. Kouprianov, A. P. LaCluyzé, D. A. Moffett, J. P. Moore, J. L. Stanley, and S. White, "The fading of Cassiopeia A, and improved models for the absolute spectrum of primary radio calibration sources," *mnras*, vol. 469, pp. 1299–1313, Aug. 2017.

[27] R. A. Perley and B. J. Butler, "An Accurate Flux Density Scale from 50 MHz to 50 GHz," *apjs*, vol. 230, p. 7, May 2017.

[28] GMRT-NCRA, "The gmrt: System parameters and current status," http://www.ncra.tifr.res.in/ncra/gmrt/gtac/next-gmrt-cycle-34/gmrt_status_doc_dec2017_v1.pdf.

[29] ——, "If deflection data cspa data summary 12jan2017 080418 1390 cyga summary," http://gmrt.ncra.tifr.res.in/~pmqc/pmqc_12jan2017/12Jan2017_080418_1390_CYGA.pdf.

Dr. Yogesh B. Karandikar has received his B. E. degree in Electronics and Telecommunication Engineering from University of Mumbai in 2004. He has received MSc degree in Radio Astronomy & Space Science in 2006 and PhD in 2012 from Dept of Microtechnology and Nanoscience both at Chalmers University of Technology, Gothenburg, Sweden. His research interests are feeds for reflectors and Lens antennas. His main focus is on Radio Astronomy Instrumentation and THz Imaging Radars. Currently he is working with Tantrayut Telecommunications where the focus is on broadband front end systems for Square Kilometer Array.

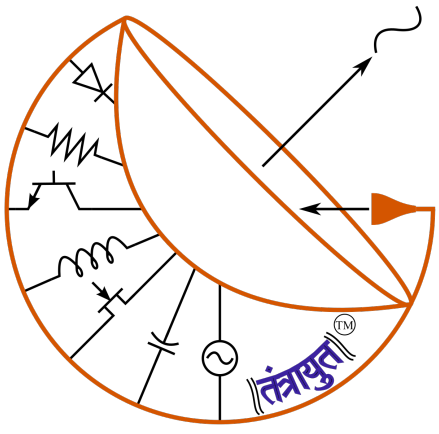

Tantrayut Telecommunications Pvt. Ltd.

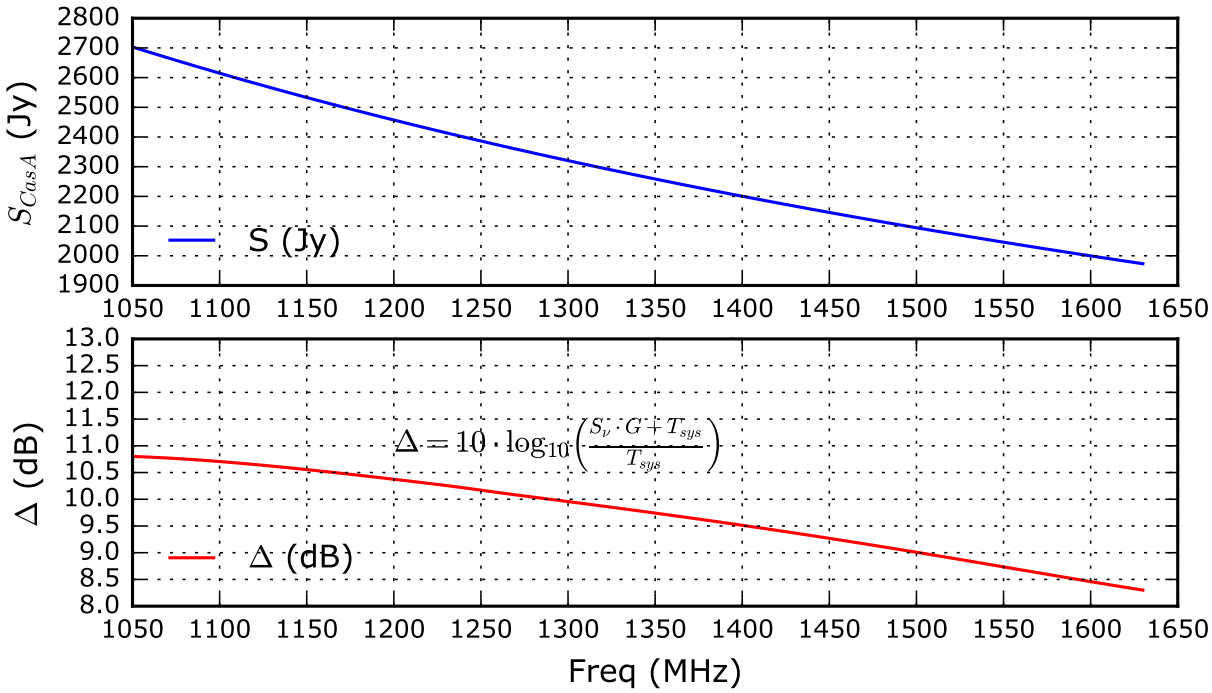

Fig. 13: CasA Source Flux and Corresponding Deflection

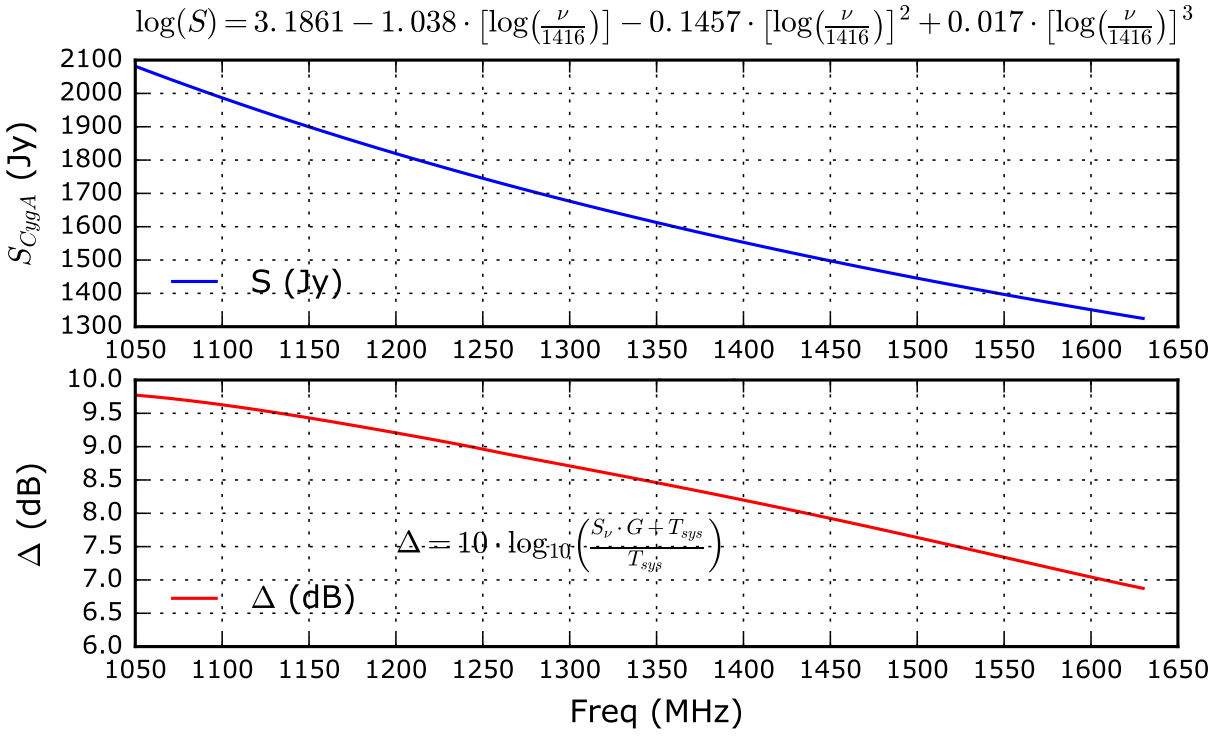

Fig. 14: CygA Source Flux and Corresponding Deflection